Toward an imaging capability with the Southern Connecticut Stellar Interferometer

Paul M. Klaucke^a, Richard A. Pellegrino^a, Samuel A. Weiss^a, and Elliott P. Horch^a

^aSouthern Connecticut State University, 501 Crescent Street, New Haven, USA

ABSTRACT

The Southern Connecticut Stellar Interferometer (SCSI) is an intensity interferometer that is designed to use correlated photon arrival times to determine the geometry of stars. Originally a low-cost, two-telescope instrument that used a 1-pixel single-photon avalanche diode (SPAD) detector at the focal plane of each telescope to record photon events, it is now being upgraded to include a third telescope. This will allow for the simultaneous detection of the photon correlation at three baselines, and thus the ability to map out the two-dimensional geometry of the source much more efficiently than with the two-telescope arrangement. Recent papers in the literature suggest that it may be possible to derive phase information in the Fourier domain from such triple correlations for the brightest stars, potentially giving SCSI an imaging capability. Prior to investigating this possibility, steps must be taken to maximize the observing efficiency of the SCSI. We present here our latest efforts in achieving better pointing, tracking, and collimation with our telescopes, and we discuss our first modeling results of the three-telescope situation in order to understand under what conditions the upgraded SCSI could retrieve imaging information.

Keywords: optical intensity interferometry, correlation interferometry, Hanbury Brown and Twiss Effect, phase recovery, image reconstruction

1. INTRODUCTION

Hanbury Brown and Twiss pioneered the field of stellar intensity interferometry (SII) in the 1950s when they found that bandwidth-limited, thermally-generated light is correlated by wave noise. ¹⁻⁴ Narrow bandwidth incoherent light generates a beat envelope that has a period on the order of the coherence time of light τ , and the amplitude and phase of the beat are correlated in time when measured at two different spatial locations. Either the intensity, which is proportional to the envelope of the beat pattern, or photon arrivals can be correlated in time since the probability of photon arrivals is proportional to intensity. Thus, the cross-correlation between photon streams received at two detectors will reveal a peak at the time difference corresponding to the path length difference between the detectors relative to the source. There is a direct relationship between the height of the cross correlation peak and the fringe visibility that is measured with amplitude interferometry. The great advantage is that no light interference or fringe pattern is actually measured, just the correlation between photon arrivals. The exact relationship between the correlation and the fringe visibility for two detectors is

$$\frac{\langle I(t, \mathbf{r})I(t + t_d, \mathbf{r} + \mathbf{b})\rangle}{\langle I(t, \mathbf{r})\rangle^2} = 1 + |v_{12}|^2,\tag{1}$$

where t is time, t_d is the time delay between the two apertures, **b** is the difference vector between the apertures, and **r** is spatial location of the first telescope.⁵ The angle brackets denote a time average of the multiplied intensities. Information about the spatial brightness distribution of the source can be ascertained by measuring the visibility v_{12} at different baselines, which is equivalent to measuring the spatial coherence of the source. The source size can be determined when a resolving baseline is found.

Since Hanbury Brown and Twiss concluded their experiments with Narrabri in the early 1970s,⁵ there has been extensive development of amplitude interferometers, which are generally more sensitive at red and near-infrared

Further author information: (Send correspondence to Paul M. Klaucke)

Paul M. Klaucke: E-mail: klaucke.paul@gmail.com

Optical and Infrared Interferometry and Imaging VII, edited by Peter G. Tuthill, Antoine Mérand, Stephanie Sallum, Proc. of SPIE Vol. 11446, 114461M · © 2020 SPIE CCC code: 0277-786X/20/\$21 · doi: 10.1117/12.2576346

wavelengths. Notable examples include the Center for High Angular Resolution Astronomy (CHARA) Array, ⁶ the Magdelena Ridge Observatory Interferometer (MROI), ⁷ the Navy Precision Optical Interferometer (NPOI), ⁸ the Sydney University Stellar Interferometer (SUSI), ⁹ and the Very Large Telescope Interferometer (VLTI). ¹⁰ However, mechanical stability of path-length differences between interferometer arms and site geometry often constrain the length of the baselines, and consequently can also limit the resolution obtained.

The great advantage of SII is that path length differences less than the coherence time of light, τ , are not detrimental to the measured correlation and corresponding visibility, whereas for amplitude interferometry, path length differences must be kept less than the wavelength of light. In effect, atmospheric turbulence and optical defects are negligible, since the time delay they introduce is much smaller than the coherence time of light. This property of SII can be exploited to image at shorter wavelengths, for example.

Another advantage of intensity interferometry is that the signal to noise ratio (SNR) of a correlation peak is not dependent on the optical filter width. If the frequency bandwidth is decreased, the photon rate decreases by the same amount the coherence time increases and the effects cancel out.⁵ This allows narrow-band imaging of stellar features that can present a challenge in amplitude interferometry. In addition, as discussed by Dever and Horch¹¹ and Horch et al.,^{12–14} light from a star can in theory be spread over an array of detector pixels with a diffraction grating to measure slightly different wavelengths. For a bright star with a high count rate, this technique can utilize photons that would otherwise be lost because of detector dead-time, and also make use of a larger range of wavelengths of light, significantly increasing signal-to-noise ratio (SNR).

There have been significant electronic advancements since Hanbury Brown and Twiss built and used Narrabri in the 1960s and 1970s. Their setup consisted of two 6.5m collectors, detectors with a time resolution of $\sim 10^{-8}$ s and quantum efficiency of 10%. Current detectors have a 5-fold increase in quantum efficiency and pico-second timing resolution. A much more sensitive interferometer can be built now than was possible in the 1970's. Alternatively, an interferometer with much smaller collectors can maintain the same level of sensitivity while allowing for a higher degree of portability.

At present, most SII research focuses on re-purposing large aperture atmospheric Cherenkov arrays, ^{15–17} although there is a group using smaller 1-m class Cassegrain telescopes. ¹⁸ Our group has focused on using 60 cm Dobsonian telescopes to make SII portable ^{12–14}, ¹⁹, ²⁰ with the Southern Connecticut Stellar Interferometer (SCSI). In this paper we report SCSI instrument upgrades as well as our plan to add a third telescope for imaging. The instrument upgrades combined with our refined observation procedure has allowed us to increase the count rates we can measure with the instrument. As a result, we now have the prospect of achieving higher signal-to-noise ratios (SNRs) in a given amount of time than we have previously obtained. We discuss in detail telescope improvements, recent observations, and the degree of correlation we have obtained. In the final sections of the paper, we describe how integrating a third telescope into our instrument will permit further capabilities, including the possibility of retrieving phase information of the source for extremely bright objects.

2. INSTRUMENT DESIGN AND IMPROVEMENTS

In its present configuration, SCSI consists of two Dobsonian telescopes, each with a 60 cm primary mirror and 2 m focal length, purchased from Equatorial Platforms of Grass Valley, CA. The telescope optics sit on rotating platforms for azimuth control and a rocker arrangement allows for motion in altitude. Originally we used two PDM series single photon avalanche detectors (SPADs) made by Micro Photon Devices that had circular active areas of diameter 50 microns; we have recently upgraded those to 100 micron diameter devices. This upgrade increases the angular diameter that the detectors subtend on the sky from 5.2 to 10.4 arcseconds. The timing resolution of the detectors is ~50 ps and the peak detection efficiency is ~50%. Each detector replaces the telescope eyepiece and sits at the focal plane. We currently have two narrow band filters that can be placed in front of the detectors: a 632.8-nm filter with a width of 1 nm (FWHM) and peak transmission 30% purchased from Newport Optics and a 532.0-nm filter with a ~3.5 nm width and a transmission of 95% purchased from Edmund Optics. Each SPAD is connected with a cable to one of our timing correlators, usually either a two channel PicoHarp or an eight channel HydraHarp, both made by PicoQuant. The correlators record the detectors' photon arrival times independently with the same central clock. The timing precision is 4 ps and 1 ps for the PicoHarp and HydraHarp, respectively. The telescopes, detectors, and the PicoHarp timing module are shown



Figure 1. The Southern Connecticut Stellar Interferometer (SCSI). The detectors sit in the eyepieces of the 60 cm telescopes and are wired to different input channels of the PicoQuant correlator. (The correlator is the white box on the computer cart.)

in Figure 1. Telescope alignment with the sky is performed with an Argo Navis, a small hand-sized computer with a simple LCD interface, purchased from Wildcard Innovations. An Argo Navis is kept on a stand attached to each telescope base, and motion of the telescope is controlled with a wireless hand paddle that communicates with the Argo Navis.

3. INSTRUMENT PERFORMANCE

Up to the present time, all observations that we have taken have been along a north-south baseline. At the start of each observation session we align the telescopes along a pre-drawn North-South line painted onto the pavement of the observation area. Then we separate the telescope by a baseline ranging from 1 to 9 m at present. Next, we laser-collimate each telescope by adjusting the primary and secondary mirrors. Then we align laser finders attached next to the telescope eyepieces to the eyepiece views so that when the eyepieces are replaced by the SPADs, we can manually sight the telescopes on objects. Next we align the telescopes with the sky using the Argo Navis; we select, identify, sight, and center a bright star in each telescope eyepiece. Then we calibrate the position with the Argo Navis computer. We repeat the previous step for a second star to create a virtual sky map that the Argo Navis uses in communication with the telescope servo motors for tracking. Once we finish alignment, we replace the telescope eyepieces with the SPADs and adjust the SPAD housing so that the detector pixels sit at the telescope foci. Then we connect the SPADs to the correlator via separate channels. We commence data collection by maximizing the detector count rates, making small manual adjustments to telescope pointing. The detectors subtend a small area, so we make small manual adjustments to tracking throughout an observation session to compensate for tracking errors. We use count rates to gauge tracking accuracy. We observed Vega (α Lyr, HR 7001), Deneb (α Cygni, HR 7924) and Polaris (α UMi, HR 424) with the SCSI on multiple nights in August, September, and October of 2020. All observations discussed here were taken at a 2.5 m baseline except once where a 9.1 m baseline was used to observe Polaris. In total, 22 hours of data were taken over 7 nights.

3.1 Count Rates

The PicoQuant software permits two ways of recording data with the timing correlators that we have. The first method is to allow the correlator to create the histogram of timing differences between events in the two channels

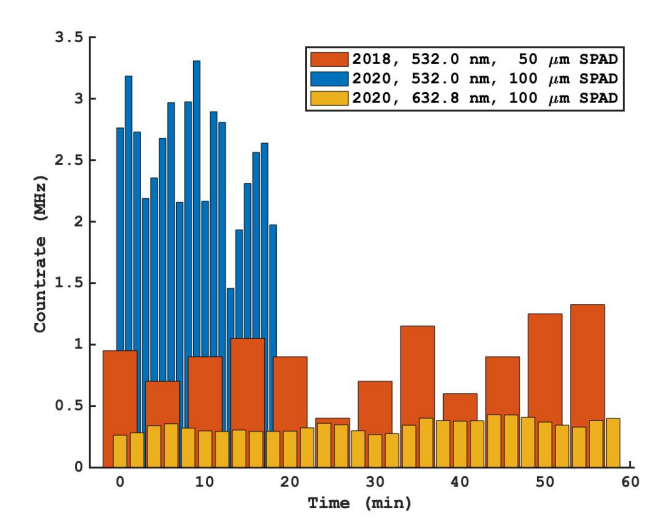


Figure 2. Count rates as a function of time for one night in 2017 when the old SPADs with 50- μ m detector area were used and two nights in 2020 when the new larger area 100- μ m SPADs were used.

in real time. In this case, the timer starts when an event is registered on the first channel and stops when an event is registered on the second channel. Then, the number of counts received in the timing bin corresponding to that timing difference is incremented by one. When the observation is complete, only the timing histogram is stored and written to a file on the host computer. The second mode is to time-tag all photons received during the observation, along with a channel identifier. In this case, each event is stored as a 4-byte data word, which is initially stored in a First-In-First-Out (FIFO) buffer, and then written in sequence to a data file. The first method is convenient for bright stars because the FIFO buffer is of limited size and high count rates can overrun it with a burst of events, whereupon the observation is terminated by the software. In general, however, the time-tagging method is more desirable for our work as it allows greater flexibility in the analysis of the data files. In either case, the original average count rate can be determined from the stored data file.

Figure 2 illustrates count rates that we have recorded in three different cases when observing Vega. The red bars indicate the average count rates observed on 21 June 2017 with the 532-nm filter and smaller detectors, that is, before the improvements discussed above were made. These data were shown in our previous work²¹ and appear here for comparison. The blue bars show the count rates achieved in 2020 with the same filter, after the system improvements were made. Finally, the orange bars show the results from 2020 using the 633-nm filter. Together, these indicate a factor of 3 improvement in the count rate obtained, and that count rates above 3 MHz are now obtainable with SCSI when observing Vega. We would also expect a decrease between the 532- and 633-nm filters of approximately a factor of nine due to the lower transmission and also the narrower bandpass of the latter, and that also appears consistent with the values in the figure.

In addition to Vega, we also observed both Deneb and Polaris using the 532-nm filter. In the case of Deneb, count rates as high as 2 MHz were briefly seen, with an average in the range of ~ 1.5 MHz, and for Polaris, the 532-nm files had an average of 0.993 MHz. Thus, what was achievable with SCSI in 2017 with Vega, namely 1 MHz, is now achievable with Polaris, a star that is 2 magnitudes fainter.

3.2 Data Reduction Strategy

We record photon arrivals in 2 or 5 minute intervals, normally using PicoQuant's time-tag mode. We choose the file length so that the change in the geometric time delay that occurs in the file due to the object's changing sky position is less than or comparable to the timing resolution of the SPAD detectors. Thus, within a single data file, most correlated photons should fall into the same timing bin when the file is used to compute the cross-correlation.

Our first step in data reduction is to split the data into "frames" of length 0.8 μ s. This time was chosen because it is the roll-over time of the PicoHarp internal clock. The cross-correlation of a frame is computed by

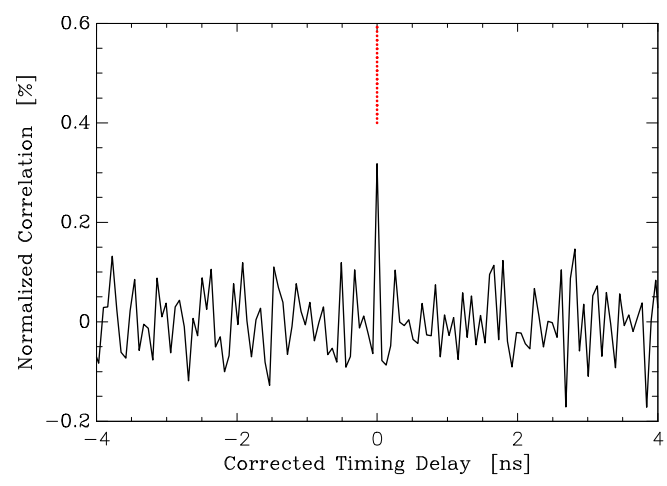


Figure 3. A cross-correlation plot made from 7.6 hours of data taken on Vega.

finding the timing difference between photon pairs, where one of the photons is received in Channel 1 and the other in Channel 2. By then creating a histogram of these timing differences, the cross-correlation is obtained. The same procedure is followed to calculate the cross-correlation of all frames in the file, and then we sum these to obtain the final cross-correlation of the file.

Once cross-correlations are formed for all data files in the observing sequence, they must be aligned in time so that the location of the correlation peak is the same. Since the star is moving in the sky as the observation sequence proceeds, the geometrical delay between the stations depends on the altitude and azimuth at the time of the observation. We average the starting and ending times for each file and compute the altitude and azimuth for that time. That is converted into a predicted timing offset for the file, which we then remove from each file prior to summing the cross-correlations obtained. Individual data files were also corrected for the small difference in cable length from the detectors to the correlator module, as measured in the lab. to the timing correlator as determined from laboratory measurements. The end result is that the peak that represents the correlation should be found at zero timing delay.

3.3 Observed Correlation Strength and Signal-to-Noise Ratio

Given the count rates that have now been achieved with the SCSI instrument, we next investigate the cross-correlation of photon arrival times between the stations. In earlier work done by our group, 21 a cross-correlation peak of significance 4.3σ above the background of random correlations was detected at the expected timing delay with SCSI when observing Vega. While the majority of the data we have taken after the improvements discussed above has yet to be thoroughly analyzed, we are in a position to add one night of data on Vega to the previous result. The resulting cross-correlation plot is shown in Figure 3. The formal significance of the peak is 4.86σ , which was achieved in a total of 7.6 hours of observing at an average count rate of 1 MHz. As expected, an overproduction of counts at zero timing delay has built up in the plot. The timing resolution used for this analysis is 64 ps per timing bin.

The background of random correlations has been subtracted in Figure 3 and the peak value represents an excess of 5590 photons in the location expected for the peak. The background value is 1.76×10^6 counts per timing bin, resulting in a normalized correlation value of 0.32 ± 0.07 %. We can compare this experimentally determined number with the theoretical value for our instrument using the signal-to-noise formula for intensity interferometry from Labeyrie, Lipson, and Nisenson, ²² namely,

SNR =
$$2.512^{-m} F_0 A \eta |v_{12}(\mathbf{b})|^2 \sqrt{\frac{T}{\Delta t}},$$
 (2)

where m is the magnitude of the star observed, F_0 is the photon flux of a zero-magnitude star times the coherence time, A is the area of a collector, η is the optical system efficiency (essentially the optical transmission times

the quantum efficiency of the detector), **b** is the baseline, v_{12} is the visibility (i.e. mutual coherence), T is the integration time, and Δt is the timing resolution of the instrument. In our case, the collection area is 0.28 m², and $v_{12}(\mathbf{b})$ is ~ 1 as we use a baseline much smaller than that which would resolve Vega (2.5 m for our set-up versus about 40 m to resolve the star). Vega's magnitude is 0.03 and that, combined with $F_0 \cdot \eta$ and the filter width must give the observed count rate of 1 MHz. Using an observation time of 7.6 hours (equal to the data set shown in Figure 3), a filter width of ~ 3.5 nm, and $\Delta t = 64$ ps, we estimate that the expected degree of correlation with the 532-nm filter is $\sim 0.43\%$. This implies that a 5σ peak would be obtained in approximately 6 hours for a count rate of 1 MHz on each detector. However, $\Delta t = 64$ ps may be an underestimate of the true timing resolution because of optical path length differences within the aperture of each telescope, which could smear out photon arrival times slightly. Small differences from night to night in the placement of the telescopes could also lead to a slightly different peak position in the timing histogram for each night, so that when coadding nights, the peak is effectively broader. We are still in the process of studying these effects, but if a Δt of 80 ps is used instead of 64 in Equation 2, then the degree of correlation is reduced to 0.38% and time needed for a 5σ peak is 7.5 hours, consistent with our experimental results.

As shown in the previous section, a 1 MHz count rate on Vega is much lower than what is now routinely measured with our instrument; in fact, we have recently obtained count rates of nearly 1 MHz on Polaris (a star of V magnitude 2.02) using the 532-nm filter. Thus, we can expect based on Figure 3 that with the efficiencies gained, we could achieve a similar plot with Polaris in roughly 8 hours of sustained observing. Since we now have substantially higher count rates on Vega, a better estimate moving forward for Vega would be to assume a 3 MHz rate on that star, in which case the observing time needed to achieve a 5σ result goes down by a factor of nine, to roughly 1 hour. However, in this case we still are not utilizing all of the light from the source because the detectors have large dead times and therefore low maximum count rates. In addition, the ability to record time-tagged data at count rates above 2 MHz has presented problems with the ability of the electronics to write the data fast enough. If we elect not to time tag but allow the timing correlator to make the cross-correlation on the fly, then the highest count rates can be used, and this is a way forward in the future with the very brightest stars, such as Vega. However, for most of the sources we wish to observe, the time-tagged mode is desirable because it allows for more flexibility in the analysis phase and count rates will be low enough to avoid the limitations experienced with Vega.

Another way to successfully observe the brightest stars is with the other filter we have at present, the 633-nm filter with 30% transmission and a 1-nm bandpass. This narrower bandpass will increase the coherence time of the wave noise, meaning that the decrease of the filter width is offset by a higher fraction of correlated events. Using Figure 3 and similar thinking to the above, we would expect a degree of correlation in that case to be about 1.9%, and a 5σ peak to be achieved in roughly 3 hours. In this case, the lower filter transmission is a disadvantage, but does offer us another viable observational pathway for Vega, and a way to check that we understand the performance of the instrument in detail by comparing the degree of correlation with that of the 532-nm filter. We do not expect to use the 633-nm filter with science observations of fainter stars at this point however.

We conclude that, for Vega, if the highest count rates obtained (about 3 MHz) can be sustained over hours of observing, then a 10- σ correlation is now potentially obtainable with SCSI in roughly 4 hours. Moving forward, our instrument will be a three-station interferometer that will record correlation peaks at three different baselines simultaneously. This opens up the possibility of having sufficient information to completely characterize a star's shape within a few nights of observing. If signal-to-noise ratios of 10 or higher can be routinely achieved at each baseline, we would have a strong motivation to further develop SCSI to do source phase recovery, and ultimately, image reconstruction.

4. PHASE RECOVERY

4.1 Theory

Progression in detector electronics and the advent of large air Cherenkov arrays, which use much of the same enabling technology as SII, have led to discussion of using SII as an imaging technique.^{23–30} Imaging with SII is not as straight-forward as imaging with amplitude interferometry, since the modulus squared of visibility

is measured and not the Fourier phase of the source brightness distribution. The phase can be recovered by measuring higher order correlations of photon arrivals at more than two telescopes. Malvimat et al.³¹ provides an expression that relates the triple correlation of photon arrivals at each telescope to the real part of the spatial bispectrum of the source brightness distribution,

$$\frac{\langle I_1 I_2 I_3 \rangle}{\langle I \rangle^3} = 1 + |v_{12}|^2 + |v_{23}|^2 + |v_{31}|^2 + 2Re[v_{12} v_{23} v_{31}],\tag{3}$$

where I_1 , I_2 , and I_3 are the intensities recorded at each measurement station. The v_{12} , v_{23} , and v_{13} terms are the fringe visibilities corresponding to the measurement station baseline pairs. The $\langle I \rangle^3$ term is the zero-baseline normalization factor. From the last term in Equation (3), the real part of the bispectrum, the cosine of the sum of the visibility phases corresponding to each baseline in the telescope triangle can be determined,

$$2\operatorname{Re}[v_{12}v_{23}v_{31}] = 2|v_{12}||v_{23}||v_{31}|\cos(\theta_{12} + \theta_{23} + \theta_{31}). \tag{4}$$

Equation (4) can be solved for the individual phases with the following result:

$$\theta_{12} + \theta_{23} + \theta_{31} = \cos^{-1} \left(\frac{|v_{12}||v_{23}||v_{31}|}{\text{Re}[v_{12}v_{23}v_{31}]} \right). \tag{5}$$

This sum of phases, also known as the closure phase, is commonly used in long baseline stellar amplitude interferometry because it is independent of telescope specific phase shift caused by atmospheric turbulence or optical defects.³²

4.2 Simulation Methods

In the coming months, we will integrate a third telescope into SCSI with the intent of observing at multiple baselines simultaneously. We now investigate under what conditions the calculation of triple correlations to potentially recover phase information can be done. Toward that end, we have developed a simulation tool to create simulated data and measure triple correlations of photon arrivals at three telescope stations. To generate photon arrivals we start by making a beat pattern for a 50-ps interval that is based on the optical filter center and width. Next, we compute the expectation value over the 50-ps interval and use the result to compute a random number from a Poisson distribution with a mean set equal to the expectation value. The result represents the expected number of photon arrivals in the interval. We repeat the previous two steps for each of the 64 elements in a frame. Although our current data processing pipeline discussed in Section 3 uses a 0.8-ms frame length, we use a shorter 3.2-ns (64 elements) frame length to shorten computation time.

We generate photon arrivals for the second and third telescope, henceforth referred to as correlator input Channels 2 and 3, based on the optical filter center, the angular source size, and the telescope baselines. At present, we use a symmetrical source for simulation, so baselines are not vectors. For zero baseline, the correlation between photon arrivals is a maximum. For this case, we sample the Poisson random number generated arrivals using the same expectation values we used for Channel 1. If a baseline is not zero, then we replace a percentage of the numbers used to make the beat pattern of Channel 1 with new random numbers. We measured correlation as a function of the number of elements replaced and fit the correlation with a close to linear second order polynomial. We call this the "elements replaced" (ER) model. For a given source size, observation wavelength, and baseline, the normalized correlation should follow a first order Bessel function for a star modeled as a uniform-disc,⁵

$$|v(\lambda, d)|^2 = \left[2\frac{J_1(\pi b\theta/\lambda)}{\pi b\theta/\lambda}\right]^2.$$
 (6)

We find the correlation using Equation (6) and then input the value into the inverse ER model to determine the number of elements to replace to make the Channel 2 and 3 beat periods. Once we make the beat periods for Channel 2 and 3, we follow the same procedure used to generate photon arrivals for Channel 1. We do not count photon arrivals if they occur within the time interval set by the previous photon arrival plus the deadtime. Once we generate all three Channels, we cross and triple correlate arrivals in each frame using the cross

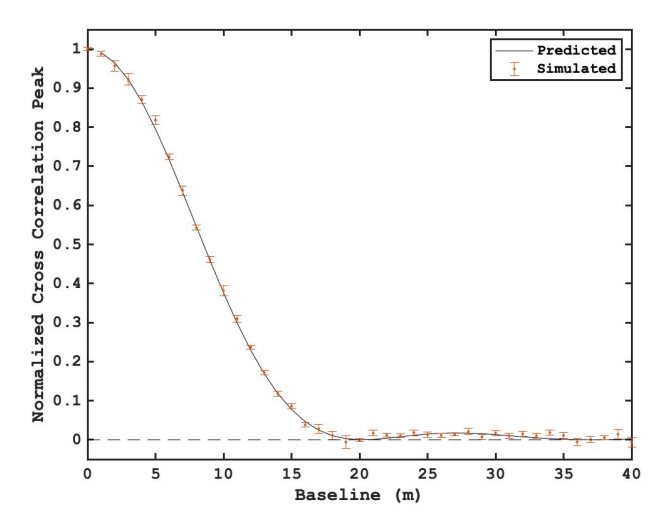


Figure 4. Simulated and predicted cross correlation peaks generated by a two station instrument are plotted as a function of baseline. The error bars represent standard error of the mean.

correlation theorem for baseline pairs and the inverse Fourier transform of the bispectrum for the three telescope combination.

Simulation of a realistic number of frames is time consuming; it takes approximately one minute to generate 20 microseconds of photon arrivals. To overcome the high time cost of generating a significant SNR, we instead use a high photon count rate (50GHz) because the SNR scales linearly with count-rate.¹³ The result is equivalent to using a low count-rate and a high integration time (many frames), but is much faster to compute.

4.3 Simulation Results

The first goal of our simulation is to show that we can produce a correlation plot for a point-symmetric source that matches theoretical expectations. We use a high count rate and a narrow filter width (0.1 nm) in place of a high integration time to simulate photon arrival correlations from Sirius. The other parameters we use to generate the results are an optical filter centered on 450 nm and a source angular diameter size of 5.6 mas to allow for comparison with Hanbury Brown and Twiss's spatial correlation measurements of Sirius. We compute the zero baseline correlation, i.e. the normalization factor, from the mean of 50 trials of 100 frame simulation runs. Most of the other correlations represent the mean of 20 trials each, but in some cases, more simulations were run to reduce the uncertainty of certain baselines. We compute the predicted correlation via Equation (6). The simulated correlations match the predicted correlation within the error bars and are also a close match to Hanbury Brown and Twiss's measurements.

The second goal of simulation is to incorporate a third station, or "channel", into the simulation so that we can study phase retrieval by triple correlating photon arrivals at the three stations. In Figure 5 we show the cross and triple correlations, respectively, of photon arrivals at three telescopes arranged in an equilateral triangle. The background levels are subtracted and the correlations are normalized by the zero baseline correlation. The simulation parameters we used to generate the data are an integration time of 40.96 μs , a baseline of 10 m, a source size of 5.6 mas, an observation wavelength of 532 nm (to match our filter center), an optical filter width of 0.1 nm and zero detector dead-time. The cross correlation and triple correlation show bright peaks for zero timing delay, as expected.

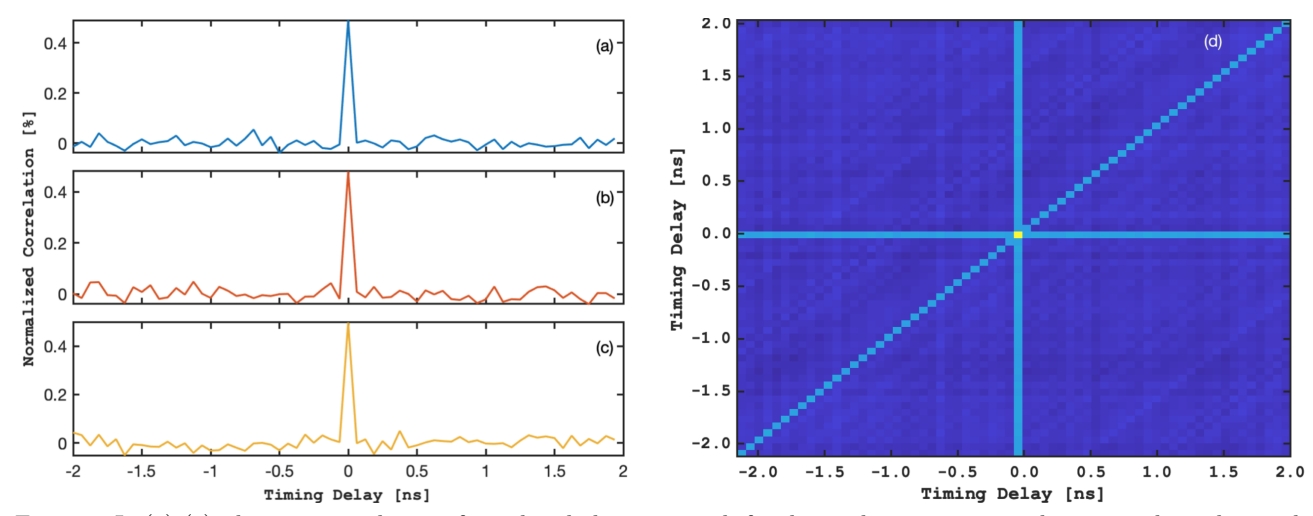


Figure 5. In (a)-(c), the cross correlation of simulated photon arrivals for three telescopes arranged in an equilateral triangle are plotted as a function of timing delay. The baselines are the same for each telescope pair. In (d), the triple cross correlation of simulated photon arrivals for three telescopes arranged in an equilateral triangle is plotted as a function of timing delay. The light blue vertical, horizontal, and diagonal lines represent temporal coherence between photon arrivals of two out of the three telescopes.

5. DISCUSSION

The third telescope being integrated into the SCSI instrument will potentially allow us to recover phase information about a source by cross- and triple-correlating photon arrivals at the three stations and then using Equations (3)-(5) to solve for the sum of the Fourier phase angles. A system of equations can then be used to solve for the individual phases in the baseline triangle. The number of baselines generated by n telescope positions (x,y) is

$$C(n,m) = \frac{n!}{m!(n-m)!},$$
 (7)

where the value of m is equal to 2, since a pair of telescopes constitutes a single baseline. The number of equations generated for n positions can be found by setting m equal to 3, which is equivalent to asking "how many triangles can be formed from n telescope positions." Five unique telescope positions (n = 5) yields 10 baselines and 10 equations; as discussed by Monnier,³² information from these equations is generally combined with additional image constraints to reconstruct images.

The dependence of image reconstruction quality on the strength and uncertainty of correlations deserves further investigation. For now, we can see how the sum of the phase angles $(\theta_{12} + \theta_{23} + \theta_{13})$ depends on the arc-cosine argument in Equation (5). If we assume an argument uncertainty of 10% and let the argument range from [-0.6, 0.6], we get an estimate of the uncertainty of the sum of the theta terms as a function of the value of the arc-cosine argument. In Figure 6, we show this by sampling a Gaussian distribution that represents the distribution of the mean of the arc-cosine argument with a standard deviation equal to 10% of the mean. We sample the distribution 10,000 times and use the samples to compute theta sums. We then measure the uncertainty of the phase sum by taking its standard deviation over the 10,000 trials and then repeat for arc-cosine mean values ranging from [-0.6, 0.6]. We use [-0.6, 0.6] as the domain to avoid sampling values that fall outside of the domain of arc-cosine ([-1,1]). Evidently, the uncertainty of the theta terms increases with the absolute value of the arc-cosine arguments. This indicates that we may improve image reconstruction quality by spending more time on correlations that yield an arc-cosine argument that is not close to zero. That being said, the complexity of a source distribution will determine how precise phase measurements need to be. For highly symmetric, low complexity source distributions, we do not expect that the precision of phase measurements will have a strong impact on image reconstruction quality. We will investigate this further with simulation.

As discussed in Section 3.3, the count rates we have seen from Vega allow us to estimate that it would take us about 4 hours to measure a 10σ cross correlation peak with our current instrument. We can extend this estimate

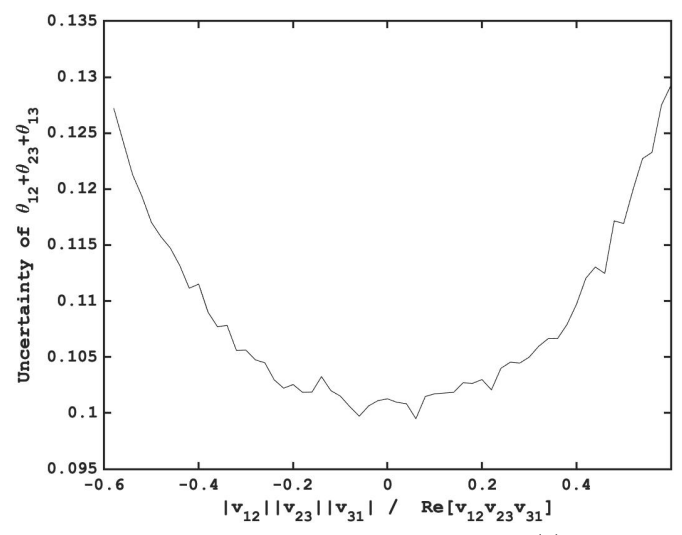


Figure 6. The uncertainty of the phase sum on the left hand side of Equation (5) is shown as a function of the arc-cosine argument on the right hand side of the equation.

to the triple correlation by using a formula provided by Malvimat et al., 31

$$SNR = |v_{123}|^2 (r\tau)^{3/2} \frac{1}{\Lambda t} \sqrt{T\tau}, \tag{8}$$

where r is the photon count rate (equivalent to $2.512^{-m}F_0A\eta/\tau$ in Equation 2), and $|v_{123}|^2$ is the normalized triple correlation. Using our 532-nm filter and assuming a width of 3.5 nm, the coherence time ($\tau = \lambda^2/c\Delta\lambda$) is equal to 0.27 ps. Using 64 ps for Δt , 10 hours for T, and 3 MHz for r, we compute a .0011 σ correlation peak. If we instead use our narrower filter with $\lambda_0 = 633$ nm, then the resulting value for the SNR is similar, since the filter has a much lower transmission. This shows that the count rates we can achieve with SCSI in its current configuration are not sufficient for phase retrieval.

However, it also points out the importance of two strategies that we can employ in the future with SCSI in order to make progress toward that goal. The first of these is to use a diffraction grating to put a sequence of distinct very narrow wavelength intervals on several SPAD devices effectively arranged in a one-dimensional pixel array. For example, if this could be done for 10 pixels, each with a 0.1-nm bandpass with 90% transmission, then the SNR calculation above becomes much more favorable. By scaling the count rates we have achieved on Vega and Polaris, we estimate that each pixel would receive approximately 7×10^5 counts per second when observing Sirius (V = -1.46). In that case, using the above equation and again assuming 10 hours of data taking, the SNR is 0.3 per pixel; if there are 10 pixels, then this becomes $0.3 \cdot \sqrt{10} \approx 1$. Therefore, phase information could potentially be retrieved with SCSI, but only over many nights of observing. The second strategy is to take SCSI's detectors and electronics to larger telescopes. If three telescopes of 2.0-m diameter are used, this increases the SNR by a further factor of roughly 10, so that phase information of Sirius could potentially be successfully obtained in one night.

6. CONCLUSION

We have recently refined the observation procedure with the Southern Connecticut Stellar Interferometer and upgraded our detectors in an attempt to make the instrument more efficient. In this paper we have presented recent observations and simulations to investigate the current capabilities of the instrument. We are now able to consistently achieve higher count rates by a factor of nearly 3 versus the performance prior to these changes. Our latest correlation results show that given the count rates we can achieve on Vega, we should be able to measure a 10σ peak in about 8 hours. With further improvements, including the addition of a third telescope, even better results could be obtained. A new simulation tool that we have developed will help us study the triple correlation of photon arrivals at three telescopes and the possibility of phase retrieval. By arranging our telescopes at five

unique positions, we can solve for the Fourier phase angles corresponding to the measured correlation peaks. If we are able to map out enough of the Fourier domain with correlations, including the phase information, it would in theory be possible to reconstruct an image of a source. However, before that becomes practical with SCSI from an observational perspective, we will need to move to a multi-wavelength approach where narrow bandpasses are recorded by a number of SPAD devices at each telescope simultaneously. With 10 pixels at each telescope and bandpasses of 0.1 nm and apertures of 2 m diameter, a $\sim 5\sigma$ peak in the triple correlation would be achievable in approximately one night of observing.

ACKNOWLEDGMENTS

We gratefully acknowledge funding from the National Science Foundation, Grant AST-1909582.

REFERENCES

- [1] Hanbury Brown, R. and Twiss, R., "Interferometry of the intensity fluctuations in light-I. Basic theory: the correlation between photons in coherent beams of radiation," *Proceedings of the Royal Society of London. Series A. Mathematical and Physical Sciences* **242**(1230), 300–324 (1957). The Royal Society London.
- [2] Hanbury Brown, R. and Twiss, R., "Interferometry of the intensity fluctuations in light IV. A test of an intensity interferometer on Sirius A," *Proceedings of the Royal Society of London. Series A. Mathematical and Physical Sciences* **248**(1253), 222–237 (1958). The Royal Society London.
- [3] Hanbury Brown, R. and Twiss, R., "Interferometry of the intensity fluctuations in light. II. An experimental test of the theory for partially coherent light," *Proceedings of the Royal Society of London. Series A. Mathematical and Physical Sciences* **243**(1234), 291–319 (1958). The Royal Society London.
- [4] Hanbury Brown, R. and Twiss, R., "Interferometry of the intensity fluctuations in light III. Applications to astronomy," *Proceedings of the Royal Society of London. Series A. Mathematical and Physical Sciences* **248**(1253), 199–221 (1958). The Royal Society London.
- [5] Hanbury Brown, R., "The intensity interferometer; its application to astronomy," iiaa (1974).
- [6] McAlister, H., Ten Brummelaar, T., Gies, D., Huang, W., Bagnuolo Jr, W., Shure, M., Sturmann, J., Sturmann, L., Turner, N., Taylor, S., and others, "First results from the CHARA array. I. An interferometric and spectroscopic study of the fast rotator Leonis (Regulus)," The Astrophysical Journal 628(1), 439 (2005). Publisher: IOP Publishing.
- [7] Creech-Eakman, M., Romero, V., Payne, I., Haniff, C., Buscher, D., Dahl, C., Farris, A., Fisher, M., Jurgenson, C., Klinglesmith, D., and others, "Magdalena Ridge Observatory interferometer: 2014 status update," in [Optical and Infrared Interferometry IV], 9146, 91460H, International Society for Optics and Photonics (2014).
- [8] Armstrong, J. T., Mozurkewich, D., Rickard, L. J., Hutter, D. J., Benson, J. A., Bowers, P., Elias II, N., Hummel, C., Johnston, K., Buscher, D., and others, "The navy prototype optical interferometer," The Astrophysical Journal 496(1), 550 (1998). Publisher: IOP Publishing.
- [9] Kok, Y., Ireland, M., Tuthill, P., Robertson, J., Warrington, B., Rizzuto, A., and Tango, W., "Phase-referenced Interferometry and Narrow-angle Astrometry with SUSI," *Journal of Astronomical Instrumentation* 2(02), 1340011 (2013). Publisher: World Scientific.
- [10] Glindemann, A., Bauvir, B., Van Boekel, R., Correia, S., Delplancke, F., Derie, F., di Folco, E., Gennai, A., Gitton, P., Huxley, A., and others, "Growing up—the completion of the VLTI," in [Scientific drivers for ESO future VLT/VLTI instrumentation], 279–288, Springer (2002).
- [11] Dever, M. and Horch, E., "An Optical System for Multi-wavelength Intensity Interferometry with the Southern Connecticut Stellar Interferometer," AAS 234, 103–03 (2019).
- [12] Horch, E., Van Belle, G., Genet, R., and Holenstein, B., "Intensity Interferometry for the 21st century," Journal of Astronomical Instrumentation 2(02), 1340009 (2013). World Scientific.
- [13] Horch, E. P., "Cutting the cord: toward wireless optical intensity interferometry," in [Advanced Photon Counting Techniques IX], 9492, 949202, International Society for Optics and Photonics (2015).

- [14] Horch, E. P., Weiss, S. A., Rupert, J. D., LaRue, R., Peronio, P., Rech, I., and Gulinatti, A., "Prospects for wireless optical intensity interferometry with the Southern Connecticut stellar interferometer," in [Optical and Infrared Interferometry and Imaging VI], 10701, 107010Y, International Society for Optics and Photonics (2018).
- [15] Abeysekara, A., Benbow, W., Brill, A., Buckley, J., Christiansen, J., Chromey, A., Daniel, M., Davis, J., Falcone, A., Feng, Q., and others, "Demonstration of stellar intensity interferometry with the four VERITAS telescopes," *Nature Astronomy*, 1–6 (2020). Nature Publishing Group.
- [16] Acciari, V., Bernardos, M., Colombo, E., Contreras, J., Cortina, J., De Angelis, A., Delgado, C., Díaz, C., Fink, D., Mariotti, M., and others, "Optical intensity interferometry observations using the MAGIC Imaging Atmospheric Cherenkov Telescopes," Monthly Notices of the Royal Astronomical Society 491(2), 1540–1547 (2020). Oxford University Press.
- [17] Matthews, N. and LeBohec, S., "Astrophysical measurements with the VERITAS Stellar Intensity Interferometer," arXiv preprint arXiv:1908.03587 (2019).
- [18] Rivet, J., Siciak, A., de Almeida, E., Vakili, F., Domiciano de Souza, A., Fouché, M., Lai, O., Vernet, D., Kaiser, R., and Guerin, W., "Intensity interferometry of P Cygni in the H emission line: towards distance calibration of LBV supergiant stars," Monthly Notices of the Royal Astronomical Society 494(1), 218–227 (2020). Oxford University Press.
- [19] Horch, E. P. and Camarata, M. A., "Portable intensity interferometry," in [Optical and Infrared Interferometry III], 8445, 84452L, International Society for Optics and Photonics (2012).
- [20] Horch, E. P., Weiss, S. A., Rupert, J. D., DiMaio, A. J., Nusdeo, D. A., Peronio, P., Rech, I., Gulinatti, A., and Giudice, A., "Scsi: the southern connecticut stellar interferometer," in [Optical and Infrared Interferometry and Imaging V], 9907, 99071W, International Society for Optics and Photonics (2016).
- [21] Weiss, S. A., Rupert, J. D., and Horch, E. P., "Stellar photon correlation detection with the Southern Connecticut stellar interferometer," in [Optical and Infrared Interferometry and Imaging VI], 10701, 107010X, International Society for Optics and Photonics (2018).
- [22] Labeyrie, A., Lipson, S. G., and Nisenson, P., [An introduction to optical stellar interferometry], Cambridge University Press (2006).
- [23] Wentz, T. and Saha, P., "Feasibility of observing Hanbury Brown and Twiss phase," Monthly Notices of the Royal Astronomical Society 446(2), 2065–2072 (2015). Oxford University Press.
- [24] Nunez, P. D., Holmes, R., Kieda, D., and LeBohec, S., "High angular resolution imaging with stellar intensity interferometry using air Cherenkov telescope arrays," *Monthly Notices of the Royal Astronomical Society* **419**(1), 172–183 (2012). The Royal Astronomical Society.
- [25] Nunez, P. D. and Domiciano de Souza, A., "Capabilities of future intensity interferometers for observing fast-rotating stars: imaging with two-and three-telescope correlations," *Monthly Notices of the Royal Astronomical Society* **453**(2), 1999–2005 (2015). Oxford University Press.
- [26] Dolne, J. J., Gerwe, D. R., and Crabtree, P. N., "Cramer-Rao lower bound and object reconstruction performance evaluation for intensity interferometry," in [Optical and Infrared Interferometry IV], 9146, 914636, International Society for Optics and Photonics (2014).
- [27] Holmes, R., Lebohec, S., and Nunez, P., "Two-dimensional image recovery in intensity interferometry using the Cauchy-Riemann relations," in [Adaptive Coded Aperture Imaging, Non-Imaging, and Unconventional Imaging Sensor Systems II], 7818, 78180O, International Society for Optics and Photonics (2010).
- [28] Holmes, R., Calef, B., Gerwe, D., and Crabtree, P., "Cramer–Rao bounds for intensity interferometry measurements," *Applied optics* **52**(21), 5235–5246 (2013). Optical Society of America.
- [29] Gerwe, D., Crabtree, P., Holmes, R., and Dolne, J., "Comparison of forward models and phase retrieval for image formation from intensity interferometer data," in [Unconventional Imaging and Wavefront Sensing 2013], 8877, 88770F, International Society for Optics and Photonics (2013).
- [30] Dravins, D., LeBohec, S., Jensen, H., Nuñez, P. D., Consortium, C. T. A., and others, "Optical intensity interferometry with the Cherenkov Telescope Array," *Astroparticle Physics* 43, 331–347 (2013). Elsevier.
- [31] Malvimat, V., Wucknitz, O., and Saha, P., "Intensity interferometry with more than two detectors?," Monthly Notices of the Royal Astronomical Society 437(1), 798–803 (2014). The Royal Astronomical Society.
- [32] Monnier, J. D., "Phases in interferometry," New Astronomy Reviews 51(8-9), 604-616 (2007). Elsevier.